Biophysical Journal
Article

Biophysical Society

How spatial temperature gradients modulate infrared stimulation of the ex vivo rat sciatic nerve

Louis Vande Perre,[1,2,*] Javier Chávez Cerda,[1] Benoit Haut,[3] Maxime Verstraeten,[1] Romain Raffoul,[1] Jean Delbeke,[4] Riëm El Tahry,[4,5] Simon-Pierre Gorza,[2] and Antoine Nonclercq[1]

[1]Bio-, Electro- and Mechanical- Systems (BEAMS), Université libre de Bruxelles, Brussels, Belgium; [2]Service Opera-Photonique, Université libre de Bruxelles, Brussels, Belgium; [3]Transfers, Interfaces and Processes (TIPs), Chemical Engineering Unit, Université libre de Bruxelles, Brussels, Belgium; [4]Institute of Neurosciences (IoNS), Université Catholique de Louvain, Brussels, Belgium; and [5]Department of Neurology, Cliniques Universitaires Saint Luc, Brussels, Belgium

ABSTRACT Infrared neural stimulation (INS) uses transient near-infrared light to activate neuronal activity, likely through heat-induced thermal gradients. However, neither the effect of basal temperature nor heat accumulation has specifically been investigated. This study examines how spatial temperature gradients, varied by different laser repetition rates and the addition of a continuous wave laser, affect the elicitation of compound nerve action potentials (CNAPs). In addition, we investigate the role of basal temperature. Overall, our results indicate that CNAP generation is more influenced by the induced spatial temperature gradients than by the increase in local or basal temperature, or temperature build-up. For instance, low-power continuous wave laser combined with low repetition rate pulsed laser stimulation successfully induced CNAPs, whereas increasing the basal nerve temperature did not facilitate CNAP generation. A heat transfer model, consistent with the experimental data, confirms that, while the volume exposed to rapid temperature changes remains constant, heat accumulation increases spatial gradients with the number of stimulation pulses. This likely explains the progressive recruitment of nerve fibers and the observed increase in CNAP amplitude. Taken together, these results highlight the critical role of spatial temperature gradients in effective infrared neural stimulation, while a temperature threshold does not appear to be the primary mechanism in CNAP triggering.

SIGNIFICANCE We developed an experimental setup in which we modulated the spatial temperature gradient imposed on an ex vivo rat sciatic nerve by using different laser stimulation repetition rates and/or a continuous wave laser. We also varied its basal temperature. The amplitude of compound nerve action potentials was increased in the presence of heat accumulation. Furthermore, we demonstrated the critical role of spatial temperature gradients in infrared neural stimulation (INS), while the temperature reached at the stimulation site may be of secondary importance in the underlying mechanism of INS. These observations contribute to efforts to understand how transient temperature changes could activate neurons in an effective and safe manner.

INTRODUCTION

Neurostimulation serves as a means to modulate nervous system activity for addressing a range of conditions such as deafness, chronic pain, neurodegenerative diseases, and epilepsy (1). Electrical stimulation has historically been the predominant method for neural activation. Yet, it suffers from various drawbacks, such as stimulation artifacts interfering with electrophysiological nerve recordings (2), imprecise spatial targeting due to current dispersion, and (3) incompatibility with magnetic resonance imaging (4). Alternative light-based neuromodulation techniques hold promise for mitigating some of these limitations (5). Among these is infrared neural stimulation (INS), a form of optical stimulation that uses transient exposure to near-infrared light to induce neural activity. Using near-infrared light to stimulate nerves obviously solves the electrical stimulation artifact issue (6). INS has been shown to be spatially selective in both the peripheral and central nervous systems (7–9). Finally, the use of light eliminates the need for metal leads, making the method compatible with magnetic resonance imaging (10).

However, the exact mechanism underlying INS remains unclear. Early studies primarily focused on photothermal

Submitted November 15, 2024, and accepted for publication March 19, 2025.

*Correspondence: louis.vande.perre@ulb.be

Editor Name: Alex Mogilner.

https://doi.org/10.1016/j.bpj.2025.03.015

© 2025 Biophysical Society. Published by Elsevier Inc.
All rights are reserved, including those for text and data mining, AI training, and similar technologies.

mechanisms, using near-infrared wavelengths at or near the local absorption maxima of water, typically 1450 nm (11), 1870 nm (12), and 2120 nm (13). More recently, the range of wavelengths studied has expanded considerably. For example, Coventry et al. demonstrated INS at 700 nm (14), which has a lower absorption coefficient, while also investigating stimulation at 1907 nm, which has a higher absorption coefficient (9). In addition, Liu et al. investigated midinfrared stimulation at 5600 nm, suggesting a possible nonthermal mechanism (15). Despite these findings, thermal mechanisms remain the most widely accepted, although alternative explanations are still being considered. Rapid heating of the nerve membrane has been proposed to induce nanopore formation (16), activate thermosensitive ion channels (17), or alter membrane capacitance (18).

Works focusing on optocapacitance, i.e., the change in membrane capacitance with light stimulation, highlighted the crucial role of a spatiotemporal temperature gradient (rather than a fixed temperature threshold) (18). They showed synchronization between temperature changes during infrared stimulation and inward currents through the cell membrane. They suggest that temperature-induced reduction in cell membrane thickness, thus increased membrane capacitance, is responsible for these inward currents and, in turn, for triggering action potentials (19). Further studies have confirmed the role of membrane capacitance in the mechanism of INS (20). Pinto et al. developed a theoretical model to describe optocapacitive current and suggested the need for fast ($<$1 ms) and localized heating of the membrane to generate action potential (21). However, given that INS has been successfully achieved with pulse durations exceeding 1 ms in various experiments (9,11,22), additional mechanisms likely contribute to neural activation beyond the optocapacitance mechanism alone.

Alternatively, Beier et al. hypothesized that INS creates temporary nanopores in the cell membrane, leading to an inward current that, in turn, generates an action potential (16). While the need for a thermal gradient in this process is suggested, uncertainty remains regarding whether it should be temporal or spatial (16).

Finally, the excitation of heat-sensitive channels, such as TRPV1 and TRPV4, has also been proposed as an INS mechanism (17,23). These thermosensitive channels are typically characterized by an activation threshold temperature that varies from 27 to over 50°C, depending on the channel type (24). Because INS is more probably triggered by a temperature change, rather than a temperature threshold, the role of heat-sensitive channels is still debated (17,23,25).

Beyond these main hypotheses for activation mechanisms, a growing diversity of proposed INS mechanisms is emerging, highlighting that multiple processes may be at play depending on wavelength and stimulation parameters. For example, Entwisle et al. demonstrated that INS can also modulate synaptic activity (26). In these in vitro patch-clamp experiments, an increase in spontaneous synaptic event frequency upon infrared irradiation is shown, even when the stimulus was insufficient to induce neuronal depolarization directly. In addition, a mechanism involving nonthermal activation of potassium ion channels was observed (15).

In parallel to the multiple works about the INS mechanism, in vivo experiments helped identify the optimal INS parameters to ensure safe and efficient neuromodulation. INS has been achieved with pulse durations in the range of microseconds (27), milliseconds (11), and seconds (28). Most agree that shorter durations are more effective (27,29–31). However, the ideal repetition rate is still debated. In addition, the spatiotemporal temperature gradient remains poorly specified. Rabbitt et al. showed that a 0.5 ms pulse duration producing a temperature increase of 0.25°C was insufficient for nerve activation, whereas a sixfold higher power pulse (same pulse duration) inducing a 1.5°C temperature increase successfully triggered a response (32). Additionally, repeated stimulation led to heat accumulation and progressive nerve inhibition. This was observed by Lothet et al. as well, and it suggests that both the spatial and temporal aspects of temperature gradients influence nerve excitability, although their precise roles were not identified, requiring further investigations (33). In the case of nerve activation, the heat accumulation caused by a sequence of light pulses at a repetition rate higher than 4 Hz resulted in nerve responses of greater amplitude (34,35). At the cellular level, Liu et al. identified two distinct thermally induced currents: one sensitive to rapid temperature changes (dT/dt) and another driven by cumulative heating (T-sensitive). The latter, which scales with heat accumulation, supports the idea that high repetition rates contribute to sustained depolarization (36). While their study did not directly assess increased sensitivity to stimulation, their results suggest that the build-up of a tonic inward current due to heat accumulation could play a role in the reduced stimulation threshold observed at higher repetition rates. However, former studies have not reported any impact of the repetition rate on the recorded compound nerve action potential (CNAP) amplitude (37–39). The potential effect of heat accumulation induced by an increased repetition rate needs to be clarified.

Here, we present a series of experiments aiming at investigating the respective role of the spatial temperature gradients as well as of the basal temperature level on the response to INS. More precisely, for a given temporal temperature gradient—linked to the peak power and pulse duration of the stimulation—we explore various spatial gradients and basal temperatures. First, INS responses were obtained over a broad range of repetition rates. Next, we performed experiments at low repetition rates but with and without the addition of a low-power continuous wave (CW) laser

to control the spatial temperature gradient. We then increased the basal temperature (i.e., the temperature of the entire nerve) to assess whether the triggering of CNAPs is dependent on the temperature reached by the nerve or whether it is predominantly influenced by local heat accumulation. Temperature measurements were also compared with simulations from a heat transfer-based nerve model to overcome the spatial and temporal limitations of the thermal imaging system and to reveal temperature gradients within the nerve.

MATERIALS AND METHODS

Fig. 1 illustrates the experimental setup designed to record CNAPs in an excised rat sciatic nerve. The setup consists of an acquisition chain for recording the electrophysiological activity of the nerve, an optical stimulator, and an electrical stimulator (for control). A halogen bulb was used to increase basal nerve temperature. In addition, a thermal camera was used to monitor the temperature at the surface of the sciatic nerve sample, allowing for the observation of spatiotemporal temperature gradients induced by INS. The experiments were performed on ex vivo rat sciatic nerve, rather than in vivo, to enable accurate monitoring of the temperature at the sample's surface, exclude interfering spontaneous electrophysiological activities, and minimize possible effects of anesthetic drugs. Experiments were performed at room temperature (except when investigating the impact of the basal temperature level) rather than at body temperature. Starting with a lower sample temperature allows to study heat accumulation and its effect on INS limiting temperatures above 43°C, where thermal damage has been observed by Wells et al. (12).

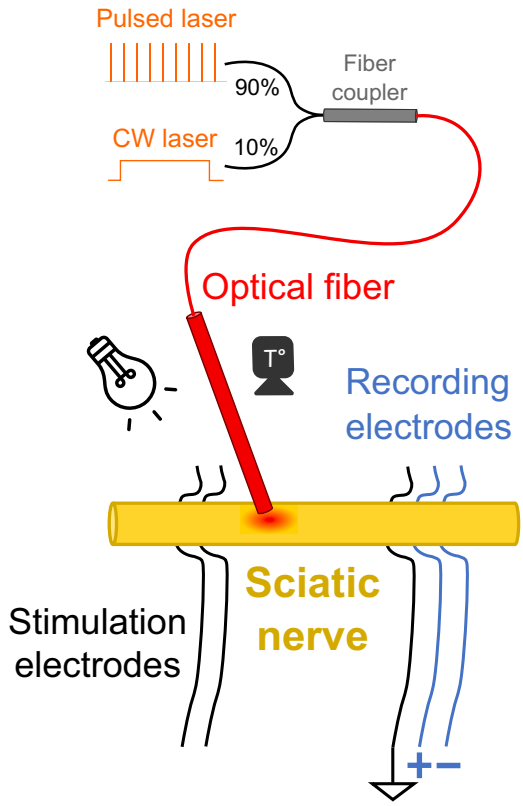

FIGURE 1 Schematic view of the experimental setup.

Electrical recording and stimulation

A custom acquisition chain was developed to record nerve electrical activity with greater modularity and sensitivity than commercially available systems. A pair of electrodes provides a bipolar recording of the electrophysiological activity of the nerve (see Fig. 1). A reference electrode is placed between the recording and stimulating electrodes to minimize the amplitude of the stimulation artifact. All electrodes are made of 99.99% silver wire with a diameter of 250 μm (Sigma-Aldrich, Hoeilaart, Belgium). Beyond the electrodes, the acquisition chain consists of a preamplifier (gain: 40 dB) followed by an amplifier (gain: 28 dB), an isolation stage (gain: −10 dB), and a filter stage (first-order high-pass, second-order Sallen-Key low-pass) with a bandwidth of 10–8000 Hz. The overall resolution of this channel is 0.20 μV with a dynamic range of $\pm$3.46 mV, both referred to the input. The measured RMS noise is 0.43 μV, also referred to the input. The amplified and filtered output is digitized by a DAQ (USB-6212, National Instrument, Austin, TX) at a sampling rate of 40 kHz. The data are processed using MATLAB (The MathWorks, Natick, MA). This recording setup is described in detail in (35,40–42).

The DAQ also interfaces with the current-controlled stimulator. The stimulator generates biphasic square current pulses (negative pulse of 0.2 ms, followed by an interphase delay of 10 μs, and finally a recovery pulse of 0.2 ms with opposite polarity) ranging from 10 to 500 μA. The same electrical stimulator has been used in (35,41).

Infrared lasers and thermal camera

The infrared laser for the optic neural stimulation is a NeoV 1470 nm pulsed diode laser from NeoLaser (Caesara, Israel). It is a compact diode laser that emits trains of light pulses with a fixed peak power (10 W) and a variable repetition rate (0.5–20 Hz). The pulse duration is set to 400 μs to deliver a pulse energy of 4 mJ to the nerve. A multimode fiber (numerical aperture 0.39, core diameter 400 μm, NeoLaser) that gently touches the surface of the nerve delivers the light to the sample (see Fig. 1).

A CW Raman laser (Raman Laser RFL-1455-40, Keopsys, Lannion, France) emitting light at a wavelength of 1455 nm was used in some experiments to control the heat accumulation irrespective of the pulse energy and repetition rate of the optical stimulation signal. A 90/10 coupler (TT400R2S2B, Thorlabs, Newton, NJ) was used to combine the output of the pulsed diode laser (90%) and the output of the CW Raman laser (10%). The combined beam (pulsed and continuous) was delivered to the nerve via a 400 μm multimode fiber with a numerical aperture of 0.39.

A GOBI-640+ thermal camera (Xenics, Leuven, Belgium) provided 640 $\times$ 480 pixel images with a maximum frame rate of 62 fps. It offers a detector NETD (noise equivalent temperature difference) of 50 mK and an integration time of 25 μs. The spatial resolution of our setup has been characterized and is equal to $\sim$0.24 mm. The thermal image was calibrated using a thermistor placed in the camera's field of view. This calibration step allows the thermal image to be independent of the lens temperature. All temperatures mentioned in the results section were extracted from the calibrated thermal image.

Surgical procedure

The experiments were conducted on sciatic nerves excised from male Wistar rats between 2.5 and 5 months old. All procedures were in accordance with a protocol approved by the Ethics Committee for Animal Experimentation at UCLouvain (2022/UCL/MD/011), in compliance with the European Convention ETS 123. The animals were housed under a 12-h day/night cycle with controlled temperature and humidity. Ad libitum access to food and water was provided. The surgery procedure described hereafter was already used in previous works (35,41,42). Anesthesia was performed with an intraperitoneal injection of ketamine (100 mg/kg body

weight) and xylazine (7 mg/kg body weight). It was maintained by bolus injections of ketamine (60 mg/kg body weight) until the animal was sacrificed. The depth of anesthesia was monitored by withdrawal reflex to noxious paw stimulation every 10 min. The surgery began with a skin incision on the lateral side of the hind limb from the knee to the hip region. The sciatic nerve was exposed after blunt dissection between the gluteus superficialis and biceps femoris muscles. The sciatic nerve was periodically irrigated with Hepes-buffered oxygenated Krebs-Ringer solution (140 mM NaCl, 5 mM KCl, 2 mM $CaCl_2$, 1 mM $MgCl_2$, 5.5 mM HEPES, 11 mM D-glucose [pH 7.3], Fisher Scientific, Brussels, Belgium) at room temperature to prevent desiccation during surgery. After the nerve was carefully dissected free of surrounding tissue, a piece of suture was tied around it as close as possible to the knee joint at one end and to the spine at the other. The nerve was then cut free beyond the sutures, leaving a 30–35 mm nerve segment tied at each extremity. The ties prevent cytoplasmic leakage and allow gentle nerve handling by holding both sutures. The nerve was then placed in an oxygenated Krebs-Ringer solution at room temperature for 20 min to allow the excised sample to recover before CNAP recordings. The solution (50 mL) was previously gassed with pure oxygen (3 L/min) for 60 min.

Ex vivo experimental protocol

After nerve excision, the sample was placed on the electrodes. The nerve was moistened with an oxygenated Krebs-Ringer solution every 5 min to prevent desiccation, but it was not immersed in the fluid. The functional state of the ex vivo samples was checked by the production of a CNAP with electrical stimulation (300 μA amplitude and 0.2 ms biphasic pulses). The experiment was stopped when the sample no longer produced CNAPs, approximately 2 h after the excision of the nerve.

The optical fiber was placed onto the nerve at a fixed position and left untouched. This is important because the recording of the nerve response to optical stimulation is sensitive to the placement of the optical fiber on the nerve. This can be explained by the high spatial selectivity of the INS (43,44). Therefore, the repetition rate and the spatial temperature gradient imposed on the nerve are the only parameters that vary in the protocol described below.

In our previous works, a sensitization effect was observed at a repetition rate of 10 Hz (35,41). In the first set of experiments, 10 Hz stimulation was performed to verify the nerve responsiveness to INS. Then, lower (2, 5, 7.7 Hz) and higher (12.5, 26.6, 20 Hz) repetition rates were applied to seven rat sciatic nerves, five of which responded, to assess the effect of repetition rate on spatial gradient and to determine how heat accumulation affects CNAP elicitation.

In the second set of experiments, performed on four rat sciatic nerves, three of which responded, the pulsed laser beam was used at a low repetition rate (2 or 0.5 Hz) to minimize heat accumulation. However, the spatial gradient observed during the 10 Hz stimulation trial was reproduced with a CW laser. The illumination power on the sample of the CW laser was thus set to 40 mW so that its average power corresponds to the 10 Hz pulse train. However, in the second half of the pulse train, the CW laser was turned off to observe the result of the dissipation of the accumulated heat on the CNAP generation.

The third set of experiments, performed on eight rat sciatic nerves, all responders, involved a uniform heating. First, the reactivity of the nerve sample to INS was tested at a repetition rate of 10 Hz with the nerve at room temperature. The nerve temperature was then uniformly increased with a halogen lamp to reach a basal temperature close to the onset temperature observed at 10 Hz (~40°C). Next, we used a 1 Hz repetition rate to test whether CNAPs could be elicited without heat accumulation, but at an elevated basal temperature. The nerve was then allowed to cool before repeating the 10 Hz stimulation to confirm the ability of the nerve to produce optically induced CNAPs. The value of 1 Hz was chosen as a good compromise between avoiding heat accumulation and a reasonable recording time.

Data analysis

All calculations and postprocessing were performed using MATLAB. The nerve response was filtered with a third-order Butterworth bandpass filter (200–1000 Hz).

To analyze the results of our experiments, we consider different temperature quantities (T_{center} and $T_{transverse}$) at key moments of the pulse train. T_{center}, which is the temperature of the pixel closest to the center of the optical spot (see, e.g., in Fig. 2 *A*). The temperature build-up, which quantifies the temperature increase caused by heat accumulation, is calculated as the difference between the local onset temperature (i.e., T_{center} before the first pulse that induced a CNAP) and the basal temperature (i.e., the average of T_{center} before the start of optical stimulation). When no CNAPs were recorded, the local maximum temperature is defined similarly to the local onset temperature, but measured before the last stimulation pulse, where its value was the greatest. Finally, regarding the spatial temperature gradient and its evolution, we considered $T_{transverse}$, measured immediately after each stimulation pulse when T_{center} reaches its maximum. The function $T_{transverse}$ is defined as the temperature of the pixels on a horizontal line (following the nerve) passing through the center of the optical spot (see Fig. 3). The spatial gradient is defined as the ratio of the peak height of $T_{transverse}$ to the full width at half-maximum, as shown in Fig. 3 *B*.

To validate the presence of CNAPs in the signal, we implemented a two-step algorithm. First, the RMS value of the signal in the 1–4 ms window following a stimulation (expected CNAP latency based on previous experiments) was compared with the baseline activity (evaluated in a window from 22 to 25 ms after stimulation time, where there is no CNAP). A CNAP was considered if its RMS value was greater than two times the standard deviation of the background window RMS (as commonly practiced in signal processing (45)). Based on this initial selection of CNAPs, a minimum of 3 epochs were averaged to obtain a smoothed version of the CNAP to serve as a template. Second, the cross correlation between a sliding window of the signal and the template was computed to quantify their similarity. A CNAP was considered present if the cross correlation of the template with a 1–4 ms window following stimulation (where a CNAP is expected) was greater than two times the standard deviation of the cross correlation of the template with the baseline signal (see Fig. 2 *E*). The CNAP onset was determined as the first CNAP of at least three consecutive CNAPs identified as genuine.

Statistical tools

The Wilcoxon signed-rank test was used for paired observations. The Wilcoxon rank sum test was used for independent sample comparisons. Because temperatures and spatial gradient measurements are expected to be higher with CNAP observations than without them, one-tailed tests were used with a 5% significance level.

Linear regression was performed using a least-squares fit of the data. The coefficient of determination (R^2) was reported to assess the goodness of fit. Additionally, the norm of the residuals (SS) is provided, as it remains informative even when the mean of the data is close to the trendline.

Heat transfer modeling

The aim of the model was twofold: first, to investigate the thermal gradient and its evolution over time inside the nerve and, second, to complement the measurements obtained with the thermal camera, which is limited in both spatial and temporal resolution.

As in our experiments, the nerve is subjected to localized periodic pulsed heating (3 s pulse train with 4 mJ pulse energy at 10 Hz repetition rate). In addition, thermal conduction within the nerve and convective/radiative exchange with the surrounding air are considered. The

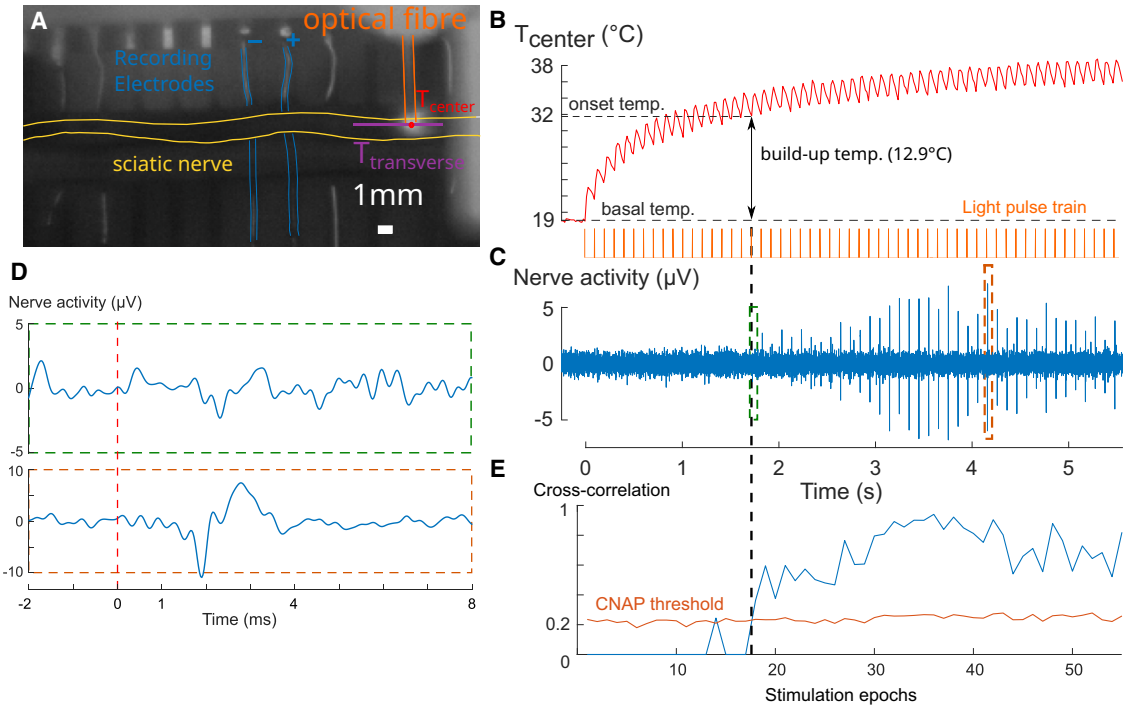

FIGURE 2 Ex vivo rat sciatic nerve stimulation: 0.4 ms pulse duration, 10 W peak power, 10 Hz repetition rate. (*A*) IR thermal camera image showing nerve temperature (brighter pixels are hotter). (*B*) Temperature at laser spot center over time (T_{center}). (*C*) Nerve electrophysiological recording from rat no. 3. (*D*) Zoom on onset (18th) and later (42nd) compound neural action potentials evoked by optical pulses (green and orange dashed boxes in *C*). Stimulation starts at t = 0. (*E*) Cross correlation in function of the stimulation epochs. The orange trace represents the threshold required to consider a CNAP genuine.

model is based on common partial differential equations (PDEs) of heat transfer, which are not fully described here but are available in the supporting material. Since the goal is mainly a qualitative comparison with the experiments, we simplified the geometry to a 2D representation while adjusting the thermal coefficient to maintain consistency with the real 3D problem. We focused on an isolated cylindrical nerve, 5 mm long and 1 mm in diameter, with the understanding that heat dissipation occurs within a confined area. The heat source was modeled as a triangle with dimensions (base of 400 μm and height of 350 μm) based on the results of photon transport modeling performed with the mcx software (46). While this approximation may not fully replicate the real-world scenario, we distributed the energy from each pulse uniformly throughout the heat source to facilitate analysis. The system of PDEs is solved using a traditional second-order discretization of the heat diffusion terms convert the PDEs into a system of ordinary differential equations in time. Wolfram Mathematica was then used to obtain the numerical solution of the ordinary differential equations over the specified time range.

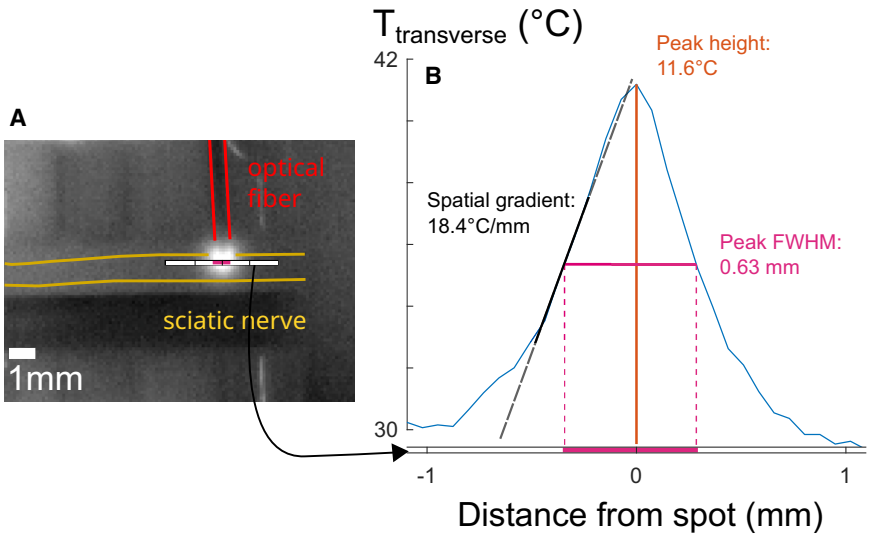

FIGURE 3 Data from rat no. 16. (*A*) Thermal image during INS showing the heat accumulation in the surroundings of the optical spot. (*B*) Temperature alongside the nerve, following the scaled line from (*A*). The spatial temperature gradient (shown with a *dashed black line*) is the ratio of the peak height to the peak full width at half-maximum (FWHM).

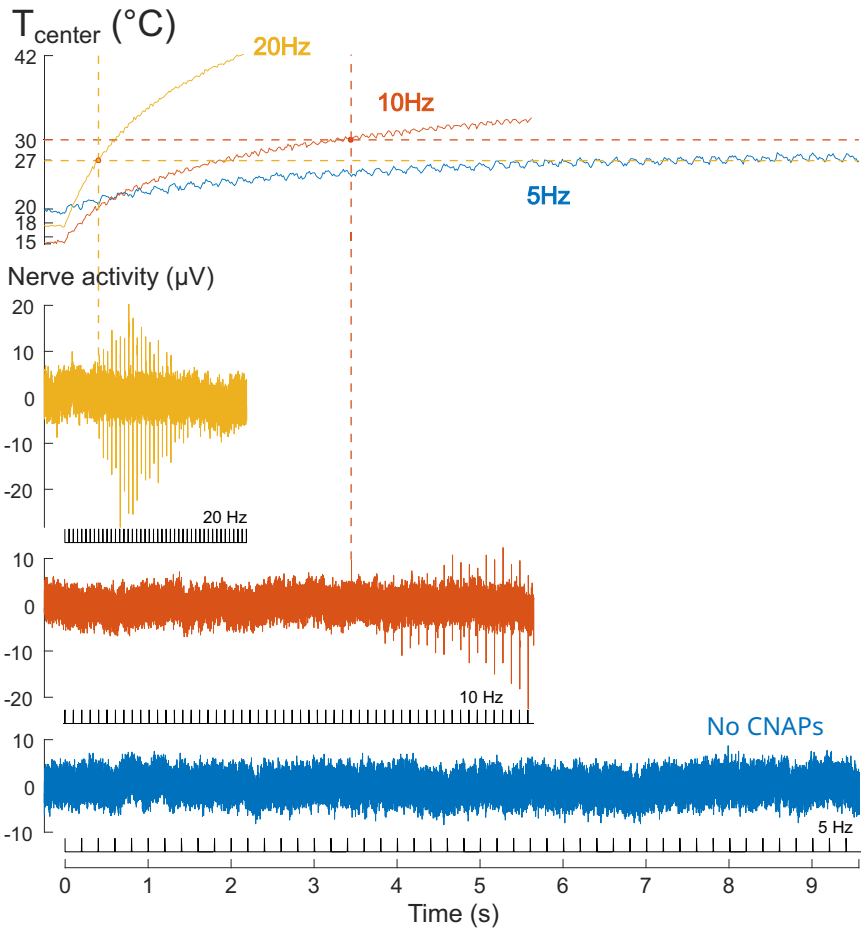

FIGURE 4 The temperature elevation and corresponding raw electrophysiological signals were recorded over 50 pulses at varying repetition rates (5, 10, and 20 Hz, indicated by pulse trains shown below each electrophysiological signals) for rat no. 5. Dashed lines indicate the onset of CNAP elicitation for each successful repetition rate.

RESULTS

Impact of the repetition rate

In previous work, we observed an increase in CNAP amplitude when using a repetition rate of around 10 Hz (35). Therefore, in this experiment, different repetition rates were used to measure the evolving spatial temperature gradient and its effect on the INS response. Fig. 2 illustrates the result of a pulse train at a repetition rate of 10 Hz with a clear sensitization effect (rat no. 3). Fig. 2 *B* shows the nerve temperature at the center of the laser spot (i.e., T_{center}) over time. The temperature increases due to the heat accumulation generated by the successive optical stimulations. Each light pulse induces a temperature jump of ∼2°C in the recorded thermal image. It should be noted that the value of the light-induced temperature peaks varies slightly from experiment to experiment, despite the constancy of the light pulse parameters. This is due to the dynamics of heat transport, which will be discussed in more detail later, and to the limited spatial and temporal resolution of the thermal imaging setup. The electrophysiological recording, presented in Fig. 2 *C*, illustrates the regular triggering of CNAPs synchronized with the light pulse delivered at a repetition rate of 10 Hz. Fig. 2 *D* (*top*) shows a closer view of the CNAP onset. Fig. 2 *D* (*bottom*) shows one of the highest amplitudes CNAP, triggered by stimulation no. 42. The CNAP amplitude increase is evident in Fig. 2 *C* and detailed in Fig. 2 *D*. As individual action potentials have a constant amplitude, the increase in CNAP amplitude corresponds to the recruitment of additional fibers by later pulses and has been termed the sensitization effect. In this specific experiment, the onset of the responses was observed after reaching a local temperature build-up of 12.9°C, corresponding to an onset temperature of 31.9°C. However, after just over 4 s of stimulation, a decrease in CNAP amplitude was observed.

In Fig. 4, we plot T_{center} over time and the associated electrophysiological signal for three different repetition rates (rat no. 5). A noticeable difference is observed between the onset and the build-up temperatures required for detecting the CNAP response. At a 10 Hz repetition rate, the CNAP emerges at stimulation no. 35, with a local onset temperature of 30.0°C and a build-up of 14.7°C. In contrast, for the 20 Hz repetition rate, the CNAP appears much sooner (i.e., at stimulation no. 9), at a local onset temperature of 26.9°C and a build-up of 9.4°C. Interestingly, the 5 Hz stimulation pulse train did not elicit a CNAP, despite a local

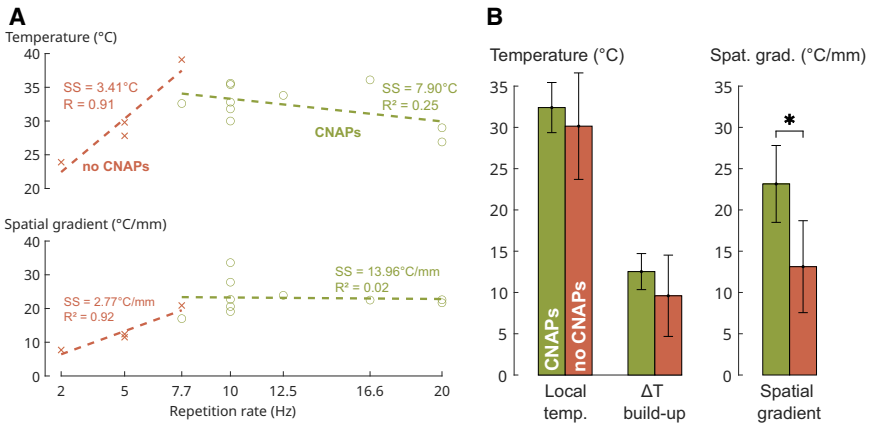

FIGURE 5 (*A*) Local temperature and spatial gradient for each optical stimulation trial as a function of repetition rate in five rat sciatic nerves. The red crosses indicate the local maximum temperature and the maximum spatial gradient reached at the end of the light pulse train for which no action potential was recorded. The green circles represent successful trials and the corresponding local temperature and spatial gradient at the onset of action potential elicitation. The dashed lines show the linear regression fitted to the data from each set. The coefficient of determination (R^2) and the norm of the residuals (SS) is given for each linear regression. (*B*) Alternative plot to compare the local temperature, the temperature build-up, and the spatial gradient between the onset of CNAP trials in successful trials (*green bars*) and the last pulse of no CNAP trials, where the highest parameter values were obtained (*red bars*). A significant difference is indicated by an asterisk ($p < 0.05$).

maximum temperature above 27°C being reached. On the other hand, the spatial gradient induced by the last pulse of the sequence at 5 Hz is 12.4°C/mm, which is much lower than the 20.6 and 22.6°C/mm measured at the onset of CNAP triggering at, respectively, 10 and 20 Hz.

A total of 14 trials were performed on 5 rats. Fig. 5 *A* shows the temperature of the optical spot and the spatial gradient as a function of the repetition rate. For unsuccessful trials (*red crosses*), local maximum temperature and maximum spatial gradient increased linearly with the repetition rate ($R^2 = 0.91$ and $R^2 = 0.92$, respectively). CNAP onset data (*green circles*) show that a 10 Hz repetition rate is necessary to record CNAPs with our setup (only one exception at 7.7 Hz). Interestingly, linear regression analysis reveals that the spatial gradient at CNAP onset remains largely independent of the repetition rate, as does the onset temperature. This is reflected in the low R^2 values ($R^2 = 0.02$ and $R^2 = 0.25$, respectively), suggesting that these parameters do not show a clear trend with the repetition rate. However, despite the low R^2, the data fit reasonably well to a horizontal trend line, as indicated by a sum of residuals that is not excessively large (SS = 13.96°C/mm and SS = 7.90°C). This suggests that, while individual variability exists, our results support the idea that a threshold gradient must be reached to observe nerve activation.

Fig. 5 *B* compares the local temperature, temperature build-up, and spatial gradient for the onset of successful trials and for the last pulse of unsuccessful trials. The local temperature and the temperature build-up were not significantly different. In contrast, the mean spatial temperature gradient required to trigger CNAPs was 23.2 ± 4.7°C/mm, significantly higher than the one in failed trials (13.1 ± 5.6°C/mm).

Overall, this series of experiments provides a first insight into the importance of the spatial temperature gradient, which should be above ∼20°C/mm to trigger a CNAP.

Effect of local heat accumulation

In this second experiment, we used low repetition rates (≤2 Hz) in the presence or absence of a CW laser, which was used to control the heat accumulation independently of the repetition rate. The CW laser was switched on synchronously with the pulsed laser stimulations. As shown in Fig. 6 *A*, CNAPs were evoked from stimulation no. 8 until the CW laser was turned off (after stimulation no. 20). Fig. 6 *B* shows the temperature profile $T_{transverse}$ at key moments of the stimulation trial. Logically, the local temperature and the build-up temperature increase with the number of pulses when the CW laser is switched on, starting at 30.1°C (stimulation no. 8) and reaching 36.7°C (stimulation no. 20). At the end of the CW heating, it decreases to 31.2°C (stimulation no. 21) but is still higher than the onset temperature. Similar observations can be drawn from the build-up temperature. In contrast, the spatial gradient varies slightly between the onset pulse (22.6°C/mm at stimulation no. 8) and the last CNAP pulse (22.9°C/mm at stimulation no. 20), but drops down to 13.6°C/mm after CW termination (stimulation no. 21). This was observed across all experiments. Fig. 6 *C* further illustrates this comparison for the three experiments conducted, showing that the local temperature and temperature build-up increase with the pulses, while the spatial gradient remains similar for the onset and the last CNAP, suggesting that the increase in CNAP amplitude is related to the heat accumulation occurring with the help of the CW laser. In addition, the local temperature and the temperature build-up are in the same range at the onset and after CW heating, while the spatial gradient decreases significantly after the CW laser is turned off, coinciding with the cessation of CNAPs.

Another exciting finding is the effectiveness of a low repetition rate, 0.5 or 2 Hz, which also induces CNAPs with progressively increasing amplitude, simultaneously with increasing heat accumulation. Globally, this second

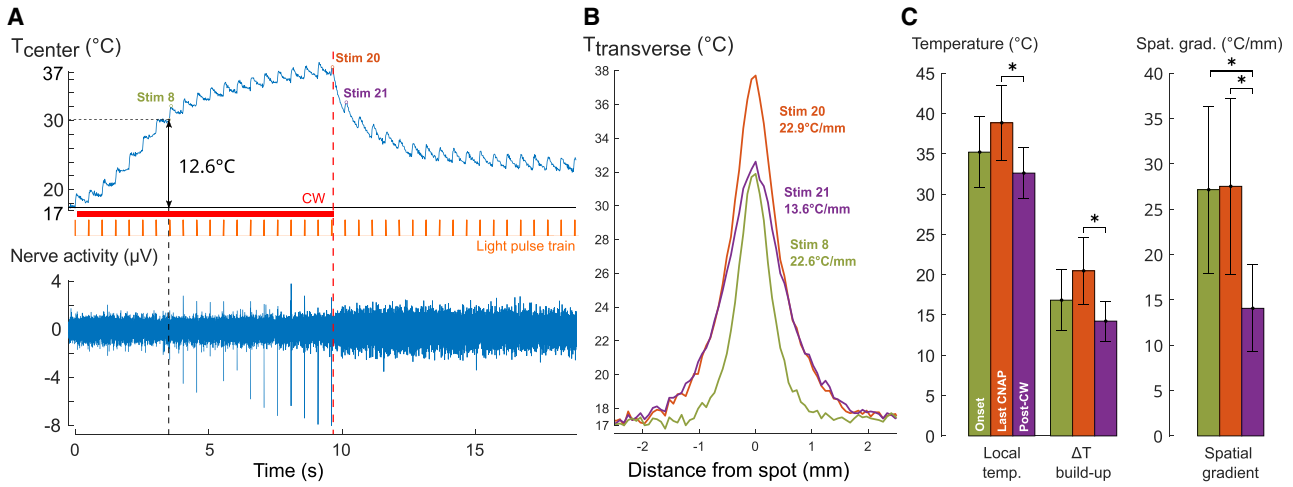

FIGURE 6 (*A*) Measured temperature increase and electrophysiological signal obtained in rat no. 6 for a sequence of about 40 pulses with a repetition rate of 2 Hz. CW laser heating is represented by the red bar, and the red dashed line marks its end. The optical pulse sequence is also shown, in orange. The black dashed line indicates the onset of the CNAP elicitation. (*B*) Temperature along the nerve for the 8th (onset), 20th (last CNAP), and 21st (post-CW) stimulation epochs. (*C*) Summary of the temperature measurements obtained during the three experiments (five stimulation trials). Data are shown in green for the onset pulse, in orange for the last CNAP and in purple for the pulse after cessation of the CW laser (resulting in the CNAP stopping). Significant differences are indicated by an asterisk ($p < 0.05$).

set of experiments suggests that the spatial gradient, rather than the repetition rate alone, is the key factor in CNAP triggering, while local temperature or temperature build-up would play a secondary role in this mechanism.

Impact of basal temperature

In this experiment, the basal temperature of the whole nerve is increased to assess whether the triggering of CNAPs is influenced by the temperature of the nerve or whether the localized temperature increase predominates over the temperature reached. Fig. 7 *A* illustrates an experiment in which a high basal temperature and low stimulation rate trial is compared with a low basal temperature and high stimulation rate (10 Hz) trial. A local temperature of 39.4°C was required to observe the first CNAP at 10 Hz. Increasing the nerve's basal temperature to 43.6°C was insufficient to evoke a CNAP with light pulses at 1 Hz. Interestingly, the temperature profiles (Fig. 7 *B*) show a very different spatial temperature gradient between these two experiments (18.4°C/mm at 10 Hz vs. 6.2°C/mm at 1 Hz).

In Fig. 7 *C*, we show these results for experiments performed on eight animals. In all experiments, CNAPs were successfully evoked at a repetition rate of 10 Hz. In contrast, in only two animals (rats 13 and 15), CNAPs were evoked at a stimulation rate of 1 Hz at a basal temperature of 35.7 and 34.4°C. In the six remaining animals, the increase in basal temperature combined with a 1 Hz repetition rate did not evoke CNAPs. The mean spatial temperature gradient of 15.69 ± 7.35°C/mm at the onset of the successful trials was significantly higher than the 5.85 ± 2.28°C/mm in the case of the absence of CNAPs during the 1 Hz stimulation trials. These results qualitatively and quantitatively emphasize the importance of the spatial gradient, over the basal temperature, in CNAP generation.

Heat accumulation modeling

We used our computational model to analyze thermal gradient evolution during INS and complement thermal imaging data obtained in our experiments. Fig. 8 *B* shows a 2D map of the simulated temperature within the nerve after 2 s of 10 Hz stimulation with a 4 mJ pulse energy. Fig. 8 *A* shows the temperature profile at a depth of 200 μm. We can see that the heat diffusion impacts the nerve temperature over a few millimeters. The surface temperatures were extracted from the simulation results (Fig. 8 *C*) and compared with experimental results. The temperature at the center of the optical spot gives us the highest temperature on the nerve (it is not measurable in a practical experiment because the optical fiber hides it). In fact, each pulse induces a temperature jump of 10°C, while our thermal imaging system only records a jump of 2°C. Therefore, in our model, we took the temperature at a distance of 1 pixel (72 μm) from the optical spot (i.e., the first pixel seen by the camera). We see then that the simulations globally agree with the measured temperatures, although heat dissipation seems to be more important in real conditions. Fig. 8 *D* shows the temporal evolution of the spatial temperature gradient at different nerve depths. Values between 10 and 22°C/mm were obtained at the surface of the nerve, similar to what was measured in the experiments. In accordance with our measurements, the spatial temperature gradient increases with time. Although the model provides qualitative information, we show in the figure the average spatial gradient required to trigger a CNAP over the 13 experiments that

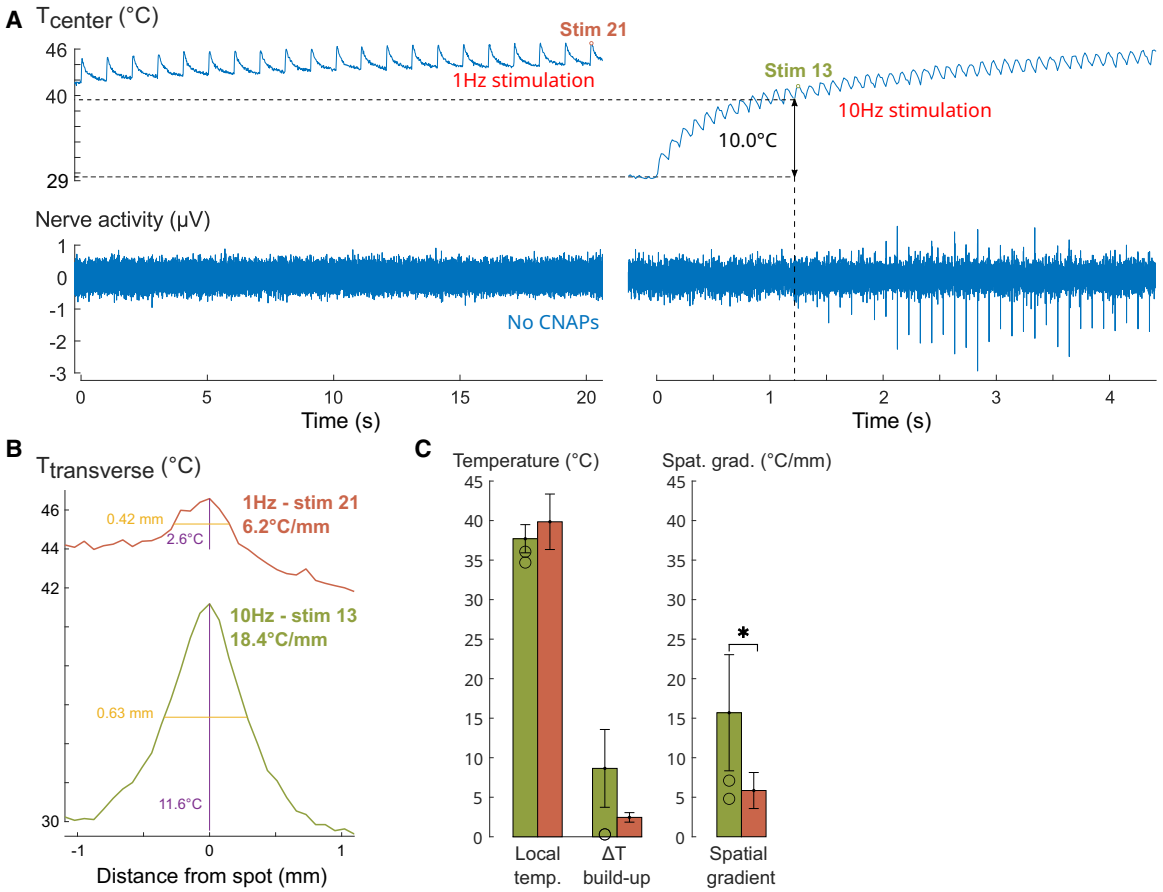

FIGURE 7 (*A*) Comparison of the temperature elevation recorded during a 1 Hz repetition rate experiment combined with increased basal temperature of the nerve sample and a 10 Hz repetition rate experiment. (*B*) Temperature profile along the nerve length for both 1 and 10 Hz repetition rate. The prominence and width of each temperature peak are respectively highlighted in purple and yellow. Data from rat no. 16. (*C*) Comparison of the local temperature, the temperature build-up, and the spatial temperature gradient while varying the basal temperature. Green bars correspond to CNAP onsets in successful trials. Red bars correspond to the highest parameter value obtained in unsuccessful trials. Note that in the latter case, the local temperature was still close to the basal temperature due to the choice of a low repetition rate to limit heat accumulation. In two animals only, represented by the circles, the stimulation with a 1 Hz repetition rate combined with increased basal temperature resulted in CNAP generation. A significant difference is indicated by an asterisk ($p < 0.05$).

we performed with a 10 Hz repetition rate. It shows that only a portion of the nerve, within a given depth and after a given stimulation time, is affected by a spatial gradient greater than 20.0°C/mm. Another interesting observation from this model is that the volume experiencing a given temperature increase (ΔT_{pulse}) is small and remains relatively constant over time, despite the cumulative heat generated during the light pulse train (as shown in Fig. 8 *E*). This result is consistent with the high spatial selectivity of the INS, as only the volume within 300 μm of the surface experiences a similar temperature change. Therefore, a combination of a rapid temperature change and an increasing spatial gradient appears to be the main cause of CNAP generation and CNAP amplitude increase.

DISCUSSION

This study investigates how spatial temperature gradients influence INS responses at a fixed pulse energy. CNAP generation was more dependent on the spatial temperature gradient than on the local temperature or heat build-up. In the 16 experiments performed, 15–35°C/mm spatial gradients were required to elicit CNAPs. Considering only the 13 experiments where 10 Hz repetition rate was used, an average spatial gradient of 20.0 ± 5.4°C/mm was measured at CNAP onset. In contrast, the local temperature or temperature build-up did not significantly differ when stimulation led to a CNAP compared with unsuccessful stimulation. Moreover, uniformly increasing the basal nerve temperature (up to 43.8°C) did not facilitate CNAP generation. Numerical simulations confirmed that, while the area exposed to significant pulse-induced temperature changes remained constant, the volume experiencing large spatial gradients increased over time, explaining the progressive recruitment of nerve fibers. These results emphasize the critical role of spatial temperature gradients in CNAP amplitude increase, while the temperature reached at stimulation may be of secondary importance.

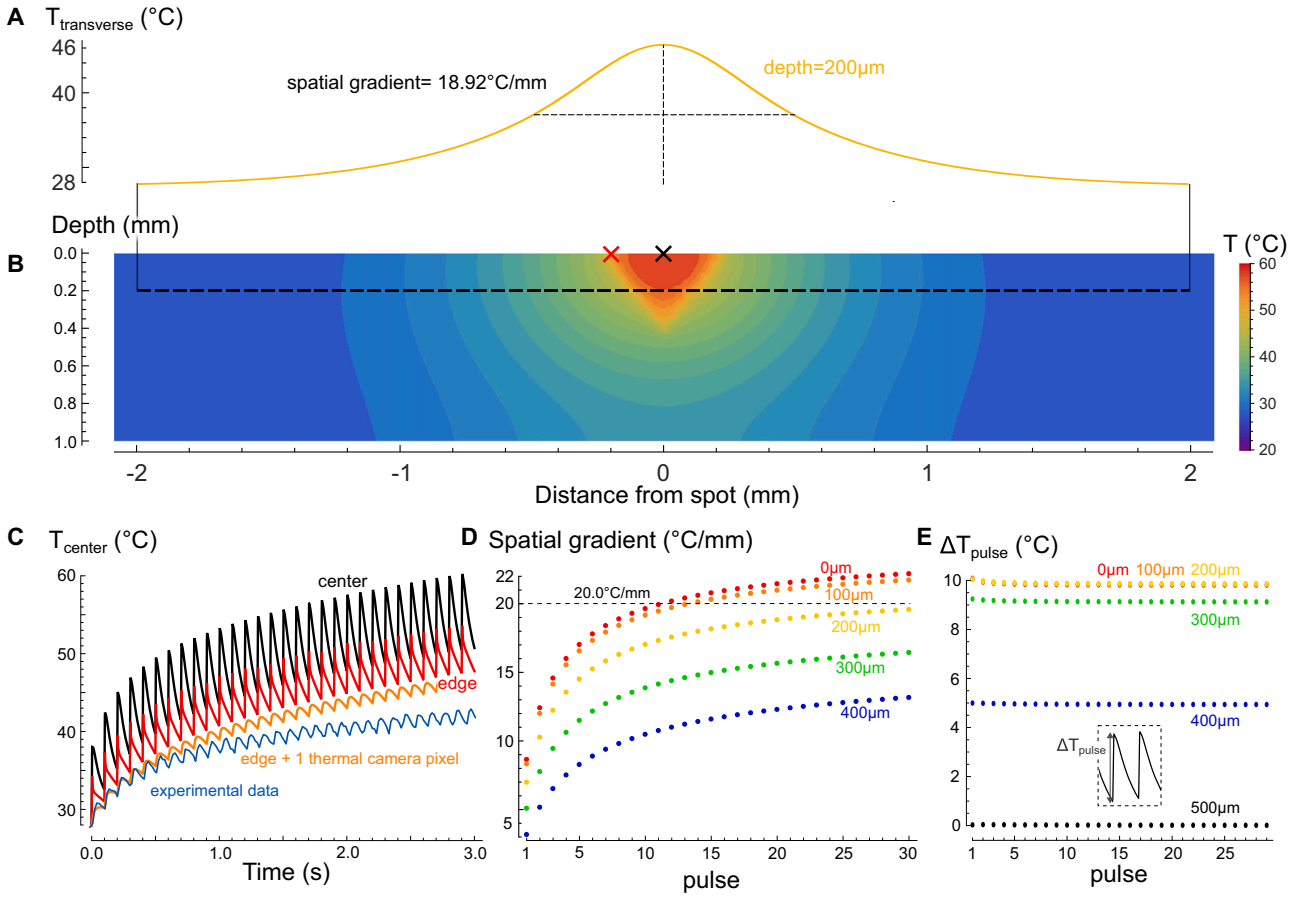

FIGURE 8 Nerve model and the associate simulations. The repetition rate is 10 Hz, and the basal temperature of the nerve is 28°C. (*A*) Temperature profile along the nerve after 2 s of stimulation (pulse no. 21) at a depth of 200 μm. (*B*) Temperatures in the nerve after pulse no. 21. (*C*) Temperature at the center of the optical spot, and at the edge of the stimulated area in function of the time. Experimental data from rat no. 16 (with an offset of minus 2°C corresponding to the basal temperature of the model). (*D*) The spatial temperature gradient in function of the number of pulses sent to the sample and at different depths in the nerve. The spatial temperature gradient is computed from the temperature profile (example in *A*) as the full width at half-maximum. The black dashed line indicates the average spatial gradient threshold, which is 20.0°C/mm computed across the 13 experiments performed with a 10 Hz repetition rate. (*E*) Temperature increase induced by each light pulse during optical stimulation. Calculated as the difference between the temperature at the end of the light pulse and the temperature before the pulse, as shown in the inset.

Impact of repetition rate and heat accumulation

We recorded CNAPs at different repetition rates. A high repetition rate (here of at least ~10 Hz) was required to trigger CNAPs, a result already obtained with ex vivo (35), in vivo, and in silico experiments (34). The latter study used a modified Hodgkin-Huxley model to account for the effect of heat accumulation and noted a decrease in stimulation threshold caused by an increased nerve basal temperature. However, our current results showed an increase in CNAP amplitude that is likely related to a spatial temperature gradient rather than an increase in basal temperature. While Izzo et al. did not report an effect of repetition rate on CNAP amplitude (37), key differences exist between their study and ours. First, they recorded from a single auditory nerve fiber in the gerbil cochlea, whereas we examined compound nerve activity in the rat sciatic nerve. Second, the cochlear nerve was immersed in a fluid, facilitating heat dissipation, potentially reducing the effects of cumulative heating we observed in our setup. Additionally, Thompson et al. used a computational model predicting minimal heat accumulation at repetition rates up to 10 Hz in the cochlear nerve (39), which may explain the lack of sensitization effects in that context.

Although few studies have investigated the sensitization effect in the context of nerve activation, similar effects have been reported in studies on nerve inhibition. Duke et al. demonstrated that heat accumulation can shape nerve activity, with high repetition rates leading to progressive conduction block (47). Similarly, Lothet et al. reported a gradual inhibition of slower nerve components under infrared stimulation, likely due to cumulative heating effects (33). These findings align with our observations and further highlight the role of thermal dynamics in INS-induced neural modulation.

A major drawback of the resulting heat accumulation is the risk of cellular damage induced by prolonged thermal

exposure. The observed decrease in CNAP amplitude at a 20 Hz repetition rate underscores the possibility of damage with excessive heat accumulation. Previous authors have warned against the possibility of thermal damage induced by heat accumulation (12,30). In our experiments, a decrease in CNAP amplitude at a repetition rate of 20 Hz was observed and is consistent with the possibility of damage from excessive heat accumulation. However, we mitigated this risk by working at room temperature during high repetition rate experiments. Even then, the temperature reached at the surface of the ex vivo sciatic nerve was still close to the identified thermal damage threshold. Therefore, a combination of functional assessment for the absence of damage (as was done in this study) and histological evaluation of the specimen is still needed to identify the safe limits of high repetition rate stimulation and the combination of CW and pulsed laser. Future work should include in vivo experiments to investigate heat dissipation into surrounding tissues.

Impact of basal temperature

In this study, we did not find any effect of the basal temperature of the nerve on its ability to generate CNAPs, which contrasts with some of the existing literature. The thermosensitive ion channel TRPV4 is known to be activated above 27°C and, thus, Albert et al. anticipated a temperature threshold as an INS triggering parameter (17). Furthermore, a modified version of the Hodgkin-Huxley model has previously demonstrated that an elevated basal nerve temperature correlates with a reduced energy threshold for electrical stimulation (34). While our results suggest that increasing the basal nerve temperature has little effect on CNAP elicitation, it is noteworthy that CNAPs were recorded in two of the eight animals, when the basal temperature was increased. This provides a nuanced perspective, suggesting that, while the temperature reached may not be as influential as expected, it may play a role. In addition, one might question the presence of TRPV4 ion channels in rat sciatic nerve, but Feng et al. demonstrated the physiological importance of these ion channels in the peripheral nervous system (48,49). However, the absence of a temperature threshold for CNAP triggering is compatible with highly compelling hypotheses of membrane optocapacitance (18) and nanoporation (16) as driving mechanisms of INS.

Temperature spatial gradient measurement and numerical modeling

Heat transfer during optical stimulation has been studied for a long time. Using a thermal camera, Wells et al. measured a temperature increase of 10–20°C in function of the pulse energy (12). Liljemalm et al. developed a numerical model for in vitro experiments and found a peak temperature of 14°C but used a smaller optical fiber diameter (100 μm) than we used (50). More recently, simulation studies of heat transfer in an axonal model during INS with a repetition rate above 5 Hz have been performed (34,51). Using a pulse energy of 4 mJ, as in our experiments, they found a temperature increase of 17.2°C after 1 s of stimulation (5 pulses) at a repetition rate of 5 Hz with their model (51). Based on the temperature profile after 5 pulses of 4 mJ, a spatial gradient of 29.7°C/mm is calculated, which is in the range of the gradients measured in our experiments. Overall, our numerical modeling is consistent with the results found in the literature. Furthermore, the combination of simulation, thermal imaging, and neural activity recording leads us to two main conclusions. First, the model confirmed the stability of the rapid pulse-induced temperature increase, independent of the local temperature. Second, we showed that the spatial gradient at a given depth increases with repeated stimuli. This means that the number of fibers experiencing a given spatial gradient increases with the number of pulses. This increase in fiber recruitment with the accumulation of light pulses could explain the increase in CNAP amplitude observed experimentally.

Limitations and further work

Recording single-nerve activity was crucial for studying CNAP generation and amplitude, particularly in relation to the spatial temperature gradient. However, CNAPs have small amplitudes, making their detection more challenging compared with the larger compound muscle action potentials commonly used in INS research (52–54). Future work could explore more selective techniques, such as inter- or intrafascicular recording (55), which may offer insights into the type of nerve fibers affected by INS, still debated (14,33,53,56). Finally, our results suggest that optimizing spatial gradients can enhance fiber recruitment and improve INS protocols. While the precise activation mechanisms remain to be fully elucidated, our results highlight the critical role of spatial gradients rather than absolute temperature increases. In particular, combining pulsed stimulation with a CW laser to modulate heat accumulation may provide a more refined approach to control nerve activation. Future studies should investigate how in vivo heat diffusion and physiological temperature regulation affect spatial gradient formation, which will be essential for optimizing INS applications in clinical settings.

DATA AND CODE AVAILABILITY

The data that support the findings of this study are available from the corresponding author upon reasonable request.

ACKNOWLEDGMENTS

Research supported by the Fonds Emile Defay. L.V.P. acknowledges the support of the Fonds pour la Formation à la Recherche dans l'Industrie

et dans l'Agriculture (FRIA, FNRS, Belgium) and the Fonds David et Alice Van Buuren. We are grateful for the help provided by Geoffrey Vanbienne in realizing our hardware setup.

AUTHOR CONTRIBUTIONS

A.N., S.-P.G., J.D., R.E.T., and L.V.P. conceived the idea for the manuscript. A.N., S.-P.G., and L.V.P. secured funding support for the published work. A.N., S.-P.G., J.D., and L.V.P. designed the experiments. R.R., J.C.C., and M.V. contributed to data processing and analysis. B.H. provided the heat transfer model and associated figures. L.V.P. performed all experiments, signal processing, data analyses, and data visualization; and wrote the manuscript. All authors contributed to editing the manuscript.

DECLARATION OF INTERESTS

J.D. reports being a shareholder of Synergia Medical SA, Belgium.

SUPPORTING MATERIAL

Supporting material can be found online at https://doi.org/10.1016/j.bpj.2025.03.015.

REFERENCES

1. Krames, E. S., P. Hunter Peckham, …, F. Aboelsaad. 2009. What Is Neuromodulation?, Volume 1. Elsevier Ltd.
2. Mcgill, K. C., K. L. Cummins, …, B. Widrow. 1982. On the Nature and Elimination of Stimulus Artifact in Nerve Signals Evoked and Recorded Using Surface Electrodes. *IEEE Trans. Biomed. Eng.* 29:129–137.
3. Liang, D. H., H. S. Lusted, and R. L. White. 1999. The nerve-electrode interface of the cochlear implant: current spread. *IEEE Trans. Biomed. Eng.* 46:35–43.
4. Manker, S. G., and F. G. Shellock. 2018. Chapter 24 - MRI Safety and Neuromodulation Systems. *In* Neuromodulation. E. S. Krames, P. H. Peckham, and A. R. Rezai, eds Academic Press, pp. 315–337.
5. Richardson, R. T., M. R. Ibbotson, …, J. B. Fallon. 2020. Optical stimulation of neural tissue. *Healthc. Technol. Lett.* 7:58–65.
6. Wells, J., P. Konrad, …, A. Mahadevan-Jansen. 2007. Pulsed laser versus electrical energy for peripheral nerve stimulation. *J. Neurosci. Methods.* 163:326–337.
7. Wells, J., M. Bendett, …, A. Mahadevan-Jansen. 2008. Frontiers in optical stimulation of neural tissues: past, present, and future. *Opt. Interact. Tissue Cells XIX.* 6854:68540B.
8. Tian, F., Y. Zhang, …, A. W. Roe. 2024. A novel interface for cortical columnar neuromodulation with multipoint infrared neural stimulation. *Nat. Commun.* 15:6528.
9. Coventry, B. S., G. L. Lawlor, …, E. L. Bartlett. 2024. Characterization and closed-loop control of infrared thalamocortical stimulation produces spatially constrained single-unit responses. *PNAS Nexus.* 3:pgae082.
10. Doguet, P., J. Garnier, …, J. Delbeke. 2024. An optoelectronic implantable neurostimulation platform allowing full MRI safety and optical sensing and communication. *Sci. Rep.* 14:11110.
11. McCaughey, R. G., C. Chlebicki, and B. J. F. Wong. 2010. Novel wavelengths for laser nerve stimulation. *Lasers Surg. Med.* 42:69–75.
12. Wells, J., C. Kao, …, E. D. Jansen. 2007. Biophysical mechanisms of transient optical stimulation of peripheral nerve. *Biophys. J.* 93:2567–2580.
13. Wells, J., C. Kao, …, A. Mahadevan-Jansen. 2005. Application of infrared light for in vivo neural stimulation. *J. Biomed. Opt.* 10:064003.
14. Coventry, B. S., J. T. Sick, …, E. L. Bartlett. 2020. Short-wave Infrared Neural Stimulation Drives Graded Sciatic Nerve Activation Across A Continuum of Wavelengths. *Annu. Int. Conf. IEEE Eng. Med. Biol. Soc.* 2020:3581–3585.
15. Liu, X., Z. Qiao, …, Y. Shu. 2021. Nonthermal and reversible control of neuronal signaling and behavior by midinfrared stimulation. *Proc. Natl. Acad. Sci. USA.* 118:e2015685118.
16. Beier, H. T., G. P. Tolstykh, …, B. L. Ibey. 2014. Plasma membrane nanoporation as a possible mechanism behind infrared excitation of cells. *J. Neural. Eng.* 11:066006.
17. Albert, E. S., J. M. Bec, …, C. Chabbert. 2012. TRPV4 channels mediate the infrared laser-evoked response in sensory neurons. *J. Neurophysiol.* 107:3227–3234.
18. Shapiro, M. G., K. Homma, …, F. Bezanilla. 2012. Infrared light excites cells by changing their electrical capacitance. *Nat. Commun.* 3:736.
19. Plaksin, M., E. Shapira, …, S. Shoham. 2018. Thermal Transients Excite Neurons through Universal Intramembrane Mechanoelectrical Effects. *Phys. Rev. X.* 8:011043.
20. Adams, W. R., R. Gautam, …, A. Mahadevan-Jansen. 2022. Visualizing the lipid dynamics role in infrared neural stimulation using stimulated Raman scattering. *Biophys. J.* 121:1525–1540.
21. Pinto, B. I., C. A. Z. Bassetto, and F. Bezanilla. 2022. Optocapacitance: physical basis and its application. *Biophys. Rev.* 14:569–577.
22. Paris, L., I. Marc, …, F. Bardin. 2017. Millisecond infrared laser pulses depolarize and elicit action potentials on in-vitro dorsal root ganglion neurons. *Biomed. Opt. Express.* 8:4568–4578.
23. Suh, E., A. D. Izzo, …, C. Richter. 2009. Optical stimulation in mice lacking the TRPV1 channel. *Proc. SPIE Int. Soc. Opt. Eng.* 7180:7180.
24. Güler, A. D., H. Lee, …, M. Caterina. 2002. Heat-Evoked Activation of the Ion Channel, TRPV4. *J. Neurosci.* 22:6408–6414.
25. Brown, W. G. A., K. Needham, …, P. R. Stoddart. 2021. Response of primary auditory neurons to stimulation with infrared light. *J. Neural. Eng.* 18:157–167.
26. Entwisle, B., S. McMullan, …, M. Withford. 2016. In Vitro neuronal depolarization and increased synaptic activity induced by infrared neural stimulation. *Biomed. Opt. Express.* 7:3211–3219.
27. Izzo, A. D., J. T. Walsh, …, C. P. Richter. 2008. Laser stimulation of auditory neurons: Effect of shorter pulse duration and penetration depth. *Biophys. J.* 94:3159–3166.
28. Yetis, O., O. Guner, …, S. Tozburun. 2021. Vagus nerve bundle stimulation using 1505-nm laser irradiation in an in-vivo rat model. *J. Biophotonics.* 15:e202100197.
29. Banakis, R. M., A. I. Matic, …, C.-P. Richter. 2011. Optical stimulation of the auditory nerve: effects of pulse shape. *Photonic Ther. Diagnostics VII.* 7883:788358.
30. Izzo, A. D., J. T. Walsh, …, C. P. Richter. 2007. Optical parameter variability in laser nerve stimulation: A study of pulse duration, repetition rate, and wavelength. *IEEE Trans. Biomed. Eng.* 54:1108–1114.
31. Throckmorton, G., J. Cayce, …, A. Mahadevan-Jansen. 2021. Identifying optimal parameters for infrared neural stimulation in the peripheral nervous system. *Neurophotonics.* 8:015012.
32. Rabbitt, R. D., A. M. Brichta, …, R. Lim. 2016. Heat pulse excitability of vestibular hair cells and afferent neurons. *J. Neurophysiol.* 116:825–843.
33. Lothet, E. H., K. M. Shaw, …, M. W. Jenkins. 2017. Selective inhibition of small-diameter axons using infrared light. *Sci. Rep.* 7:3275.
34. Alemzadeh-Ansari, M. J., M. A. Ansari, …, M. Haghjoo. 2019. Influence of radiant exposure and repetition rate in infrared neural stimulation with near-infrared lasers. *Lasers Med. Sci.* 34:1555–1566.
35. Cury, J., L. Vande Perre, …, A. Nonclercq. 2021. Infrared neurostimulation in ex-vivo rat sciatic nerve using 1470 nm wavelength. *J. Neural. Eng.* 18:056018.
36. Liu, Q., M. J. Frerck, …, R. D. Rabbitt. 2014. Exciting cell membranes with a blustering heat shock. *Biophys. J.* 106:1570–1577.

37. Izzo, A. D., P. Littlefield, …, C.-P. Richter. 2007. Laser stimulation of auditory neurons at high repetition rate. *Opt. Interact. Tissue Cells XVIII.* 6435:64350R.

38. Goyal, V., S. Rajguru, …, C. P. Richter. 2012. Acute Damage Threshold for Infrared Neural Stimulation of the Cochlea: Functional and Histological Evaluation. *Anat. Rec.* 295:1987–1999.

39. Thompson, A. C., S. A. Wade, …, P. R. Stoddart. 2013. Infrared Neural Stimulation : Influence of Stimulation Site Spacing and Repetition Rates on Heating. *IEEE Trans. Biomed. Eng.* 60:3534–3541.

40. Smets, H., L. Stumpp, …, A. Nonclercq. 2021. Analysing vagus nerve spontaneous activity using finite element modelling. *J. Neural. Eng.* 18:56008.

41. Vande Perre, L., J. Cury, A. Nonclercq…, 2022. A Setup for Conduction Velocities and Temperature Gradients Measurements during Infrared Neurostimulation. *In* 2022 IEEE Biomedical Circuits and Systems Conference (BioCAS). Taipei, Taiwan IEEE, pp. 453–457.

42. Cury, J., H. Smets, …, S.-P. Gorza. 2022. Optical Birefringence changes in myelinated and unmyelinated nerves: a comparative study. *J. Biophotonics.* 15:e202200028.

43. Duke, A. R., H. Lu, …, E. D. Jansen. 2012. Spatial and temporal variability in response to hybrid electro-optical stimulation. *J. Neural. Eng.* 9:036003.

44. Peterson, E. J., and D. J. Tyler. 2014. Motor neuron activation in peripheral nerves using infrared neural stimulation. *J. Neural. Eng.* 11:016001.

45. Fisher, R. A. 1925. Statistical Methods for Research Workers. Oliver and Boyd, Edinburgh, Scotland.

46. Fang, Q., and D. A. Boas. 2009. Monte Carlo Simulation of Photon Migration in 3D Turbid Media Accelerated by Graphics Processing Units. *Opt. Express.* 17:20178–20190.

47. Duke, A. R., M. W. Jenkins, …, E. D. Jansen. 2013. Transient and selective suppression of neural activity with infrared light. *Sci. Rep.* 3:2600.

48. Feng, X., X. Song, and M. Tominaga. 2021. Physiological Significance of TRPV4 Channels in Non-Myelinating Schwann cells. *Int. J. Phys. Med. Rehabil.* 9:1000588.

49. Feng, X., Y. Takayama, …, M. Tominaga. 2020. Increased TRPV4 expression in non-myelinating Schwann cells is associated with demyelination after sciatic nerve injury. *Commun. Biol.* 3:716.

50. Liljemalm, R., T. Nyberg, and H. Von Holst. 2013. Heating during infrared neural stimulation. *Lasers Surg. Med.* 45:469–481.

51. Ansari, M. A., and M. Zakeri. 2019. Blind localization of heating in neural tissues induced by a train of the infrared pulse laser. *J. Lasers Med. Sci.* 10:264–267.

52. Dautrebande, M., P. Doguet, A. Nonclercq…, 2018. Peripheral nerve recruitment curve using near-infrared stimulation. *In* Optogenetics and Optical Manipulation 2018 SPIE, p. 104820V.

53. Cargill, R., T. Baumann, and S. L. Jacques. 2008. Optical stimulation of excised murine sciatic nerve using 1.8-μm wavelength laser. *Opt. Interact. Tissue Cells XIX.* 6854:68540I.

54. Throckmorton, G. A., W. Thayer, …, A. Mahadevan-Jansen. 2023. Infrared neural stimulation markedly enhances nerve functionality assessment during nerve monitoring. *Sci. Rep.* 13:4362.

55. Larson, C. E., and E. Meng. 2020. A review for the peripheral nerve interface designer. *J. Neurosci. Methods.* 332:108523.

56. Vande Perre, L., J. Chávez Cerda, …, A. Nonclercq. 2025. Differences in Conduction Velocities of Nerve Fibers Excited by Infrared and Electrical Stimulation. *J. Neurosci. Methods.* 418:110427.